Article

Design of Amphibious Vehicle for Unmanned Mission in Water Quality Monitoring Using IoT

Balasubramanian Esakki[1], Surendar Ganesan[1], SilambarasanMathiyazhagan[1], G. R. Kanagachidambaresan[2], BhuvaneshwaranGnanasekaran[3], Byungrak Son[4*], Su Woo Park[5], Jae Sung Choi[6]

1 Centre for Autonomous System Research,VelTech Rangarajan Dr. Sagunthala R&D Institute of Science and Technology, Avadi, Chennai, India
2 Department of Computer Science Engineering, VelTech Rangarajan Dr Sagunthala R&D Institute of Science and Technology, Avadi, Chennai, India
3 UCAL System Ltd., Chennai, India
4 Convergence Research Center for Wellness, DGIST, Daegu, Republic of Korea
5 Rovitek Inc, Gyungsan-si, Gyungsangbuk-do, Republic of Korea
6 Sun Moon University Chungcheongnam-do, Republic of Korea
* Correspondence: brson@dgist.ac.kr, Tel.: +82-53-785-4772

Abstract: Unmanned Aerial Vehicles (UAVs) have gained significant attention in recent times due to their suitability to a wide variety of civil, military and societal missions. Development of an unmanned amphibious vehicle integrating the features of a multi-rotor UAV and a hovercraft is focus of the present study. Components and subsystems of the amphibious vehicle are developed with due consideration on aerodynamic, structural and environmental aspects. Finite element analysis (FEA) on static thrust conditions and skirt pressure are performed to evaluate the strength of structure. For diverse wind conditions and angles of attack (AOA), computational fluid dynamic (CFD) analysis is carried out to assess the effect of drag and suitable design modification is suggested. A prototype is built with a 7 kg payload capacity and successfully tested for stable operations in flight and water-borne modes. Internet of Things (IoT) based water quality measurement is performed in a typical lake and water quality is measured using pH, dissolved oxygen (DO), turbidity and electrical conductivity (EC) sensors. The developed vehicle is expected to meet functional requirements of disaster missions catering to the water quality monitoring of large water bodies.

Keywords: Amphibious UAV; Hovercraft; FEA; CFD; Prototype, Water quality, Sensors, Internet of Things

---

1. Introduction

The UAVs categorized based on the performance characteristics of wing movement as fixed-wing, rotary and flapping-wing configurations [1].Various applications of UAVs include surveillance, traffic monitoring, active weapon engagement, wild-life survey, pollution monitoring and precision agriculture etc. [2]. Authors of this paper contributed to the development of UAVs for environmental monitoring [3], structural health monitoring [4] and also constructed micro aerial vehicles [5-7]. Dedicated efforts on development of amphibious vehicles scare. Collins [8] described the importance of amphibious UAV in diverse applications and discussed issues pertaining to control, communication and airspace management of the same. Boxerbaum et.al. [9] developed robotic amphibious vehicle using the concepts of biological inspired animals to navigate in underwater and rough terrains. Yayla et. al. [10] performed theoretical analysis to investigate the

Preprints (www.preprints.org) | NOT PEER-REVIEWED | Posted: 18 September 2018 doi:10.20944/preprints201809.0326.v1

Peer-reviewed version available at Sensors 2018, 18, 3318; doi:10.3390/s18103318

performance characteristics such as rate-of-climb, turn radius and maximum velocity of amphibious UAV. Pisanich and Morris [11] fabricated sea plane conceptual model of amphibious UAV for a 4 kg payload. Autonomous flight missions are performed in air and water as a proof of concept. Hasnan and Wahab [12] designed a UAV which can fly in air, glide along land and water surface. Frejek and Nokleby [13] designed a four-paddle wheel amphibious vehicle with ultrasonic sensors to detect obstacles. The published data indicates that development of amphibious UAVs for deployment in water quality assessment is not evident from the literature. For quality evaluation of large and inaccessible water bodies, amphibious vehicle provides effective and rapid solutions. Development of a UAV that can land and glide on water surface while collecting water samples offers several challenges related to materials, energy management, control systems and on-board sensors. Present study integrates features of a multi-rotor UAV with hovercraft and this configuration for an amphibious UAV is not attempted till date. The vertical-take-off and landing (VTOL) functionality is also integrated into the system so that resultant amphibious vehicle offers several functional advantages such as energy efficient movement on water surface, eliminating of large areas for landing and take-off besides ensuring compatibility with wide variety of payloads.

2. Evolving Conceptual Model

The conceptual model is formulated integrating the multirotor and hovercraft configurations wherein four co-axial propellers and motors that are attached to the frame act as an Octo-rotor as shown in Figure 1. The entire rotor assembly is supported by a hull made of high density polyurethane foam and nylon impregnated with urethane is attached beneath for functioning as a skirt. Provision for pay loads, batteries, sensors, electronic accessories, flight controller board (FCB), water sampler with robotic arm module and water collection tanks are made in such a way that Centre of Gravity (CG) of the vehicle is maintained for stable flight.

The co-axial propellers are actuated during vertical take-off and landing. After landing on water surface, any two co-axial propellers are rotated through 90^0 using a servo motor and these propellers produce thrust for forward movement of the vehicle. Buoyancy of the vehicle is achieved through cushioning effect of the skirt produced using a duct fan. Hover gap of 2-5 mm is maintained between the skirt of amphibious vehicle and water surface. During hovering mode, all four co-axial motors are powered to create lift. In addition to design requirements, following performance specifications are considered for selection of aircraft components:

Preprints (www.preprints.org) | NOT PEER-REVIEWED | Posted: 18 September 2018 doi:10.20944/preprints201809.0326.v1

Peer-reviewed version available at Sensors 2018, 18, 3318; doi:10.3390/s18103318

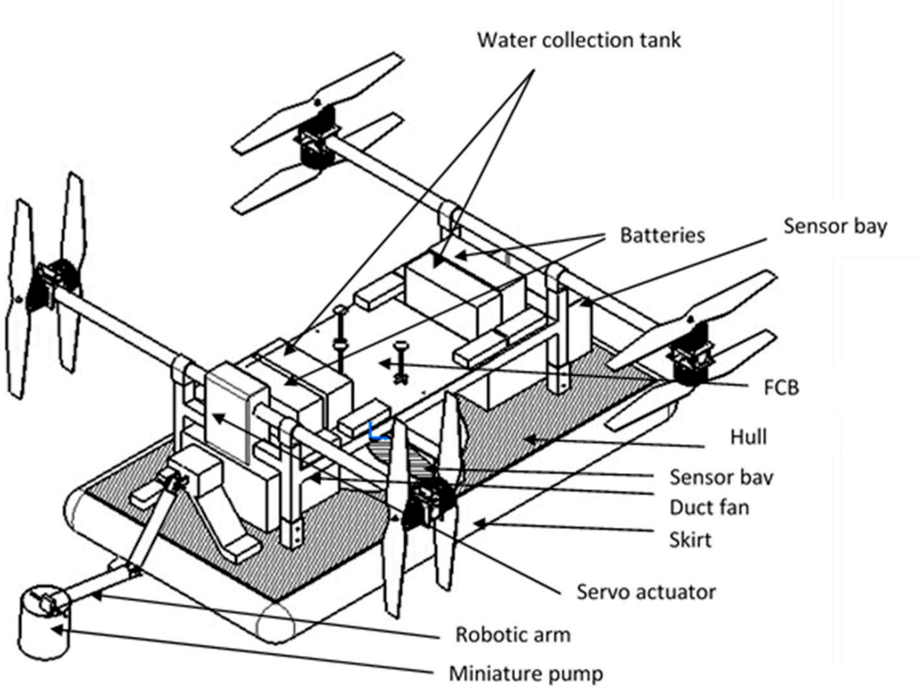

Figure 1, Conceptual Model of Amphibious Vehicle

Airborne operation

- Flight endurance of 20 mins
- Payload of 7 kg
- 40 km/hr cruise speed
- 2000 m of flight range

Hovering and moving on water body

- Endurance of 40 mins
- 30 km/hr cruise speed
- 2000 m range

Based on these design requirements and performance criteria, a mission profile for collection of water samples in remote water body locations is identified. The typical mission profile has flight conditions of VTOL, hovering on air, landing on water bodies, propelling along the water surface and vertical landing. Sequence of these missions is varied according to the operational need.

3. Design Process

Design process of the amphibious vehicle capturing the functionalities corresponding to aerodynamics, structures and compliance to performance criteria is presented in Figure 2.

Preprints (www.preprints.org) | NOT PEER-REVIEWED | Posted: 18 September 2018 doi:10.20944/preprints201809.0326.v1

Peer-reviewed version available at Sensors 2018, 18, 3318; doi:10.3390/s18103318

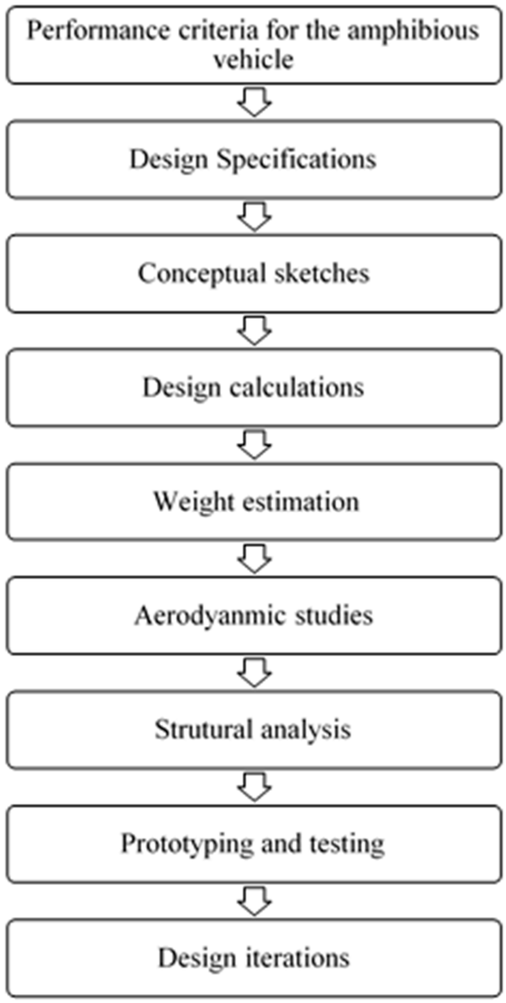

Figure 2, Design strategy of the amphibious vehicle

3.1. Design of Hovercraft

Hovercraft is an air cushion vehicle to move over the multiple terrains including land, water and muddy surfaces. The duct fan located at the centre produces necessary cushioning effect through forcing air down and creating air cushion between skirt and water surface. Inflation of skirt increases air pressure that acts at the base of hull. Forward motion of hovercraft is achieved through propelling the co-axial rotors. Since the skirt is considered to be a sensitive part of the hovercraft to achieve lift of the vehicle, selection of skirt material is an important aspect which is discussed in the following section. In order to design a hovercraft, various parameters have to be determined. Table 1 presents the list of assumptions incorporated to perform design calculations and in Table 2, hovercraft parameters are estimated for flow analysis [14].

Table 1, Assumptions of hover craft parameters

Sl. No	**Empirical relation**	**Limit**
1	Length to width (l/w)	2
2	Bag pressure to cushion pressure (P_b / P_c)	1.3
3	Forward thrust to overall weight during hovering (T_f / W)	0.2
4	Propeller pitch to diameter (p / d)	0.6
5	Vertical thrust to maximum take-off weight (T_v / W)	2

Preprints (www.preprints.org) | NOT PEER-REVIEWED | Posted: 18 September 2018 doi:10.20944/preprints201809.0326.v1

Peer-reviewed version available at *Sensors* **2018**, *18*, 3318; doi:10.3390/s18103318

Table 2, Calculation of hovercraft parameters

Parameter	Empirical relation	Values
Maximum take-off weight (W)	$m \times g$	269.78 N
Length of the hovercraft (l)	$2 \times w$	1.00 m
Cushion Area (A_c)	$l \times w - \pi r^2$	0.40 m^2
Cushion pressure (P_c)	$\frac{W}{A_c}$	674.44 N/m^2
Air escaping velocity (V_e)	$\sqrt{2\frac{P_c}{\rho}}$	33.18 m/s
Air escaping area (A_e)	$2 \times (l + w) \times h$	0.038 m^2
Air flow rate (Q_e)	$A_e \times V_e$	1.26 m^3/s
Power required (P_e)	$\frac{Q_e \times \rho \times {V_e}^2}{2}$	852.32 N

3.1.1. Selection of Skirt Material

The inflation of skirt functionality for realization of hovering and the skirt material should have sufficient tensile strength. Survey of various skirt materials of hovercraft given in Table 3 reveals that, nylon impregnated with urethane is the best choice due to high tensile strength, light weight and superior resistance to wear and tear characteristics.

Table 3, Mechanical properties of skirt

Property	**Nylon impregnated with urethane**	**Naturalrubber coated nylon**	**Vinyl-coated 1000 denier polyester**
Tensile strength (MPa)	45	35	3.06
Elastic modulus (MPa)	1.48	1.10	20.00
Density (kg/m^3)	900	1016	1500
Hardness	75	34	87
Flexural strength(MPa)	41	20	26

3.1.2. Selection of Hull Material

Hull is considered to be water tight body of hovercraft and it has to support various payloads, battery and other electronic systems. It has to withstand upward high pressure generated through cushion of air during inflation of skirt. Based on the survey of materials options (Table 4), polyurethane foam is selected due to high strength to weight ratio.

Table 4, Mechanical properties of hull

Property	**Composite Material**	**Fiber glass**	**Polyurethane foam**
Tensile strength (MPa)	1200	1950	1900
Compressive strength(MPa)	866	4000	48
Elastic modulus (GPa)	45	72	4

Peer-reviewed version available at Sensors 2018, 18, 3318; doi:10.3390/s18103318

Density (kg/m³)	7850	2540	1390
Flexural strength (MPa)	146	110	57

3.2. Multicopter Design

A hollow square cross section aluminium channel is considered for the horizontal and vertical frames for supporting the pair of motors. Speed and thrust of the motors are calculated (Table 5) using empirical relations.

Table 5, Multi-rotor structure parameters

Parameters	Empirical relation	Values
Required motor speed (N)	$\sqrt{\dfrac{L_m \times 10^{10}}{p \times d^3 \times 0.0283495 \times g}}$	4200 rpm
Thrust per motor (T)	$p \times d^3 \times N^2 \times 10^{-10} \times 0.0283495 \times g$	92 N
Lift required for multi-copter (L_m)	$2 \times W$	540 N

Lm - multicopter lift required; p - propeller pitch and d - propeller diameter; g – acceleration due to gravity

3.2.1. Propulsion

As per the initial estimation of speed of the motor, motor is selected with reference to the kv rating (125kv) having a power of 1900 W. Table 6 illustrates the necessary current rating and number of cells of a battery for 25 mins of endurance for a battery capacity of 22,000 mAh.

Table 6, Propulsion system parameters

Parameters	Empirical Relation	Values
Speed of motor (N)	$kV \times V$	4800 rpm
Operating current (I)	$\dfrac{P}{V}$	50 A
Number of battery cells (nS)	$\dfrac{V}{3.7}$	10
Endurance (E)	mAh x 0.001 x 60 / Σ I_m	25 mins

kV - motor mating; V - operating voltage; P - motor power; mAh - milliampere hour; Im – summation of current consumption

3.2.2. Selection of Propeller

Weight of amphibious system is considered to be 30 kg for selection of the propellers. A Quad with co-axial motor – propeller configuration is considered due to the demand of high payload carrying capacity and stability of vehicle. Considering thrust to weight ratio as two and 20% thrust loss due to co-axial configuration, the maximum thrust is estimated as 75 kg. At full throttle condition, propellers of various diameters and their thrust force characteristics are examined (Figure 3). In order to lift 75 kg, each co-axial arms needs to produce approximately 18.5 kg of thrust. Hence, a co-axial propeller configuration with diameter 0.75–0.80 m is selected.

Preprints (www.preprints.org) | NOT PEER-REVIEWED | Posted: 18 September 2018 doi:10.20944/preprints201809.0326.v1

Peer-reviewed version available at *Sensors* **2018**, *18*, 3318; doi:10.3390/s18103318

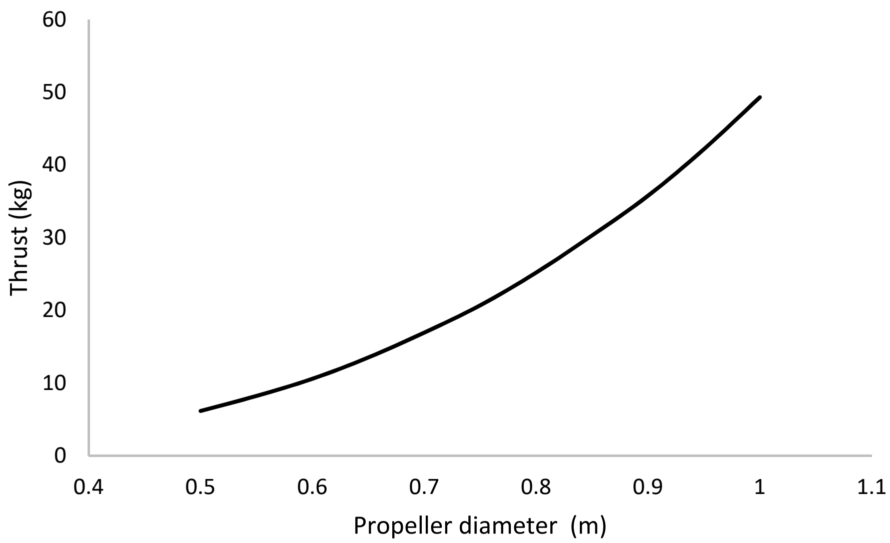

Figure 3, Selection of co-axial propeller diameter

3.2.3. Selection of Motor

Selection of motor primarily depends upon the size of the propeller for generating sufficient thrust and the selected configuration demands 10 kg thrust force per motor. Power consumption of the 125 kv motor under various speeds is determined as shown in Fig. 4. At full throttle condition, maximum power of 1.86 kw is required per each motor at a speed of 4480 rpm.

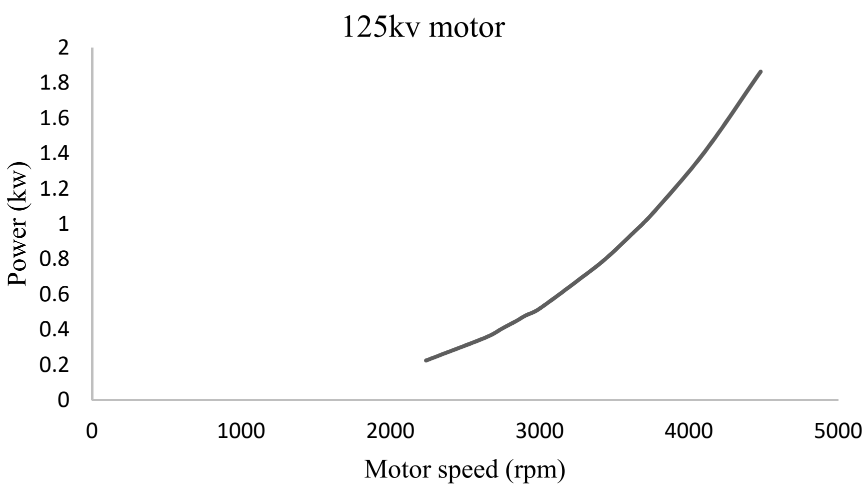

Figure 4, Power consumption characteristics of selected motor

3.2.4. Selection of Battery

Selection of battery depends upon the consumption of current with sufficient voltage and discharge rate requirements. Total current consumption for the electronic components is calculated as 2.73 Amps (Table 7). Considering 8 motors, the total power and current required for the vehicle to fly in the air are estimated as 3.78 kw and 79.13 Amps (Table 8) respectively. However, when the vehicle lands on water and glides along the water surface, two pairs of motors need to be actuated. Estimation of current and power consumption during the gliding of vehicle on the water surface is given in Table 9 and it is evident that only half of the power is required for amphibious mode as compared to flight mode.

Table 7, Estimation of power and current of on-board electronics

Sl.NO	Component Name	Power required (W)	Current Consumption (A)
1	Flight controller board	16	0.34
2	ESC	40	0.83
3	Video telemetry	15	0.34
4	Camera	10	0.21
5	On board processor	50	1.01
	Total	131	2.73

Table 8, Power consumption (Airborne mode)

Sl.No	Components	Power (W)	Total Power Consumption (W)	Total Current Consumption (A)
1	Electronics components	95.30	95.30	2.73
2	Motors (8 Nos)	460.80	3686.40	76.40
		Total	3781.70	79.13

Table 9, Power consumption (Gliding on water)

Sl.No	Components	Power (W)	Total Power Consumption (W)	Total Current Consumption (A)
1	Electronics components	95.30	95.30	2.73
2	Motors (4 Nos)	240.00	1920.00	40.00
3	Ducted Motor	100.00	100.00	2.08
		Total	2115.30	44.81

In order to meet these power and current consumption requirements, a 22000 mAh capacity battery is selected. It is expected to have estimated endurance of 22 minutes while in air flight and 46 minutes during hovering or gliding along the water body.

3.3. Weight Estimation

Based upon earlier selection of materials for hovercraft and multirotor components, weight of the amphibious vehicle is estimated as 27.31 kg inclusive of 7 kg payload. Table 10 shows the weight of various components of hovercraft and multirotor systems.

Table 10, Weight of each components

Sl. No.	Components	Weight (kg)
1	Multicopter Frames (Aluminum Alloy 6061)	1.40

Peer-reviewed version available at Sensors 2018, 18, 3318; doi:10.3390/s18103318

2	Hull (Polyurethane foam)	0.80
3	Skirt (Nylon impregnated with urethane)	1.70
4	Control system	0.45
5	Multicopter motor	3.36
6	Multicopter propeller	0.31
7	Multicopter Electronic Speed Controller (ESC)	0.88
8	Servo	0.50
9	Electronic Duct fan (EDF)	0.40
10	EDF ESC	0.11
11	Li-Po Batteries	10.00
12	Miscellaneous	0.40
13	Payload	7.00
	Total Weight	27.31

4. Structural analysis of amphibious vehicle

Multirotor configuration has vertical and horizontal frames which are made of aluminium channels owing to its light weight characteristics. At the tip of the horizontal frames, motor and co-axial propellers are attached. The vertical frames are anchored to the top surface of hovercraft hull. Thrust produced by the propellers is considered to be acting at the fixed support of horizontal frame and the same vertical axial loading is applied at the four corners of the horizontal frame. An axial load is applied at the tip of frame and the effect of cushion pressure generated through the duct fan located at the centre of hull is analysed. The pressure load is applied at the inner surface of skirt and bottom of the hull. Effect of these loading conditions is evaluated through structural analysis. Displacement of 0.6 mm is experienced at the tip of horizontal frame (Figure 5). The von-Mises stress plot (Figure 6) shows that the junction of horizontal and vertical frames experiences maximum stress regions about 25 MPa. Other portions of amphibious structure experience considerably lower level.

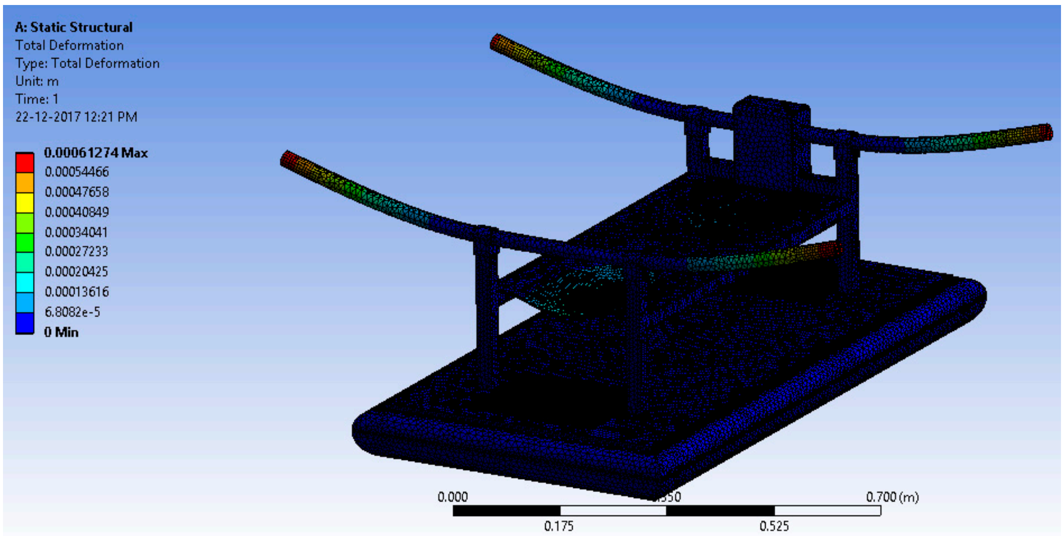

Figure 5, Deformation plot of amphibious structure

Preprints (www.preprints.org) | NOT PEER-REVIEWED | Posted: 18 September 2018 doi:10.20944/preprints201809.0326.v1

Peer-reviewed version available at *Sensors* **2018**, *18*, 3318; doi:10.3390/s18103318

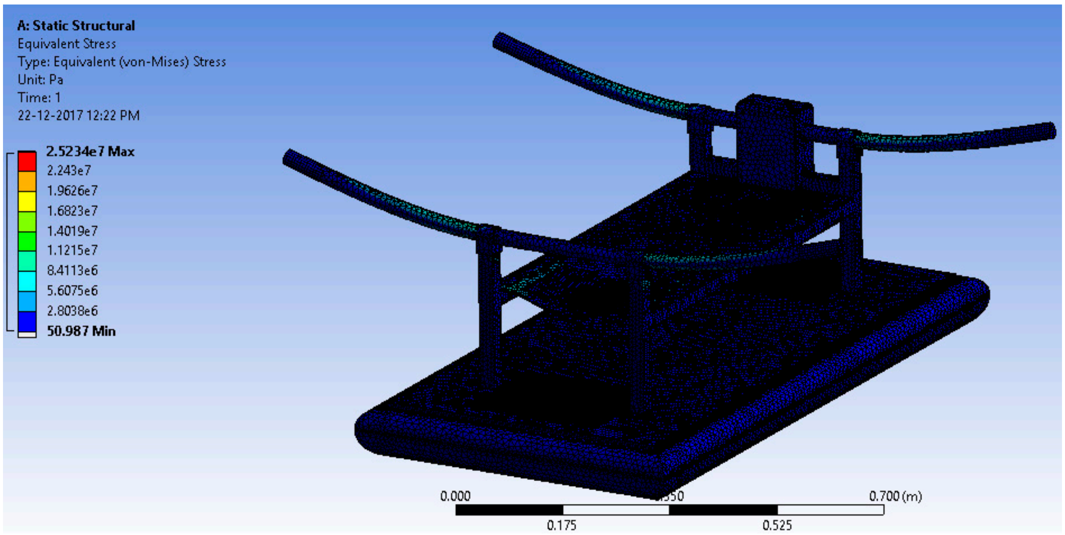

Figure 6, Stress contour of amphibious structure

5. Aerodynamic analysis

Aerodynamic evaluation of amphibious vehicle is performed through varying the wind speeds in the range of 5 to 10 m/s with different angles of attack (AOA) (0º and 8º). Computational fluid dynamic (CFD) analysis using ANSYS FLUENT platform is used to examine the velocity and pressure contours during forward flight conditions and also aerodynamic co-efficients are determined. Quality of meshing (Figure 7) is evaluated through performing orthogonality and skewness characteristics (0.9). Inlet as velocity and outlet as a pressure is considered and boundaries are defined far away (10 times) to reduce horizontal buoyancy effect and wall inference. Symmetry plane and no heat transfer are assumed to perform simulations.

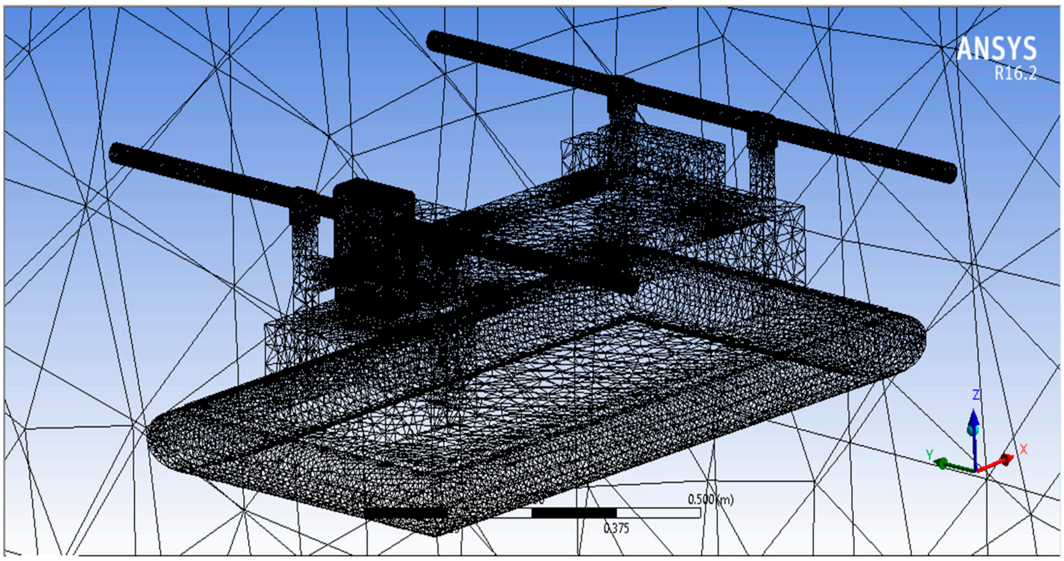

Figure 7, Meshed geometry

Simulation results indicated that at various angle of attack collision of air with frontal body surface causes velocity drop (Figure 8) due to stagnation pressure (Figure 9) and there is a loss of kinetic energy. At the middle of amphibious vehicle low pressure region is formed that creates vortex and flow separation. This phenomenon may create unbalance of the vehicle which can be streamlined through providing riblets. At the rear of vehicle recirculation flow occurs due to non-uniformity and blunt profile of UAV structure.

Preprints (www.preprints.org) | NOT PEER-REVIEWED | Posted: 18 September 2018 doi:10.20944/preprints201809.0326.v1

Peer-reviewed version available at *Sensors* **2018**, *18*, 3318; doi:10.3390/s18103318

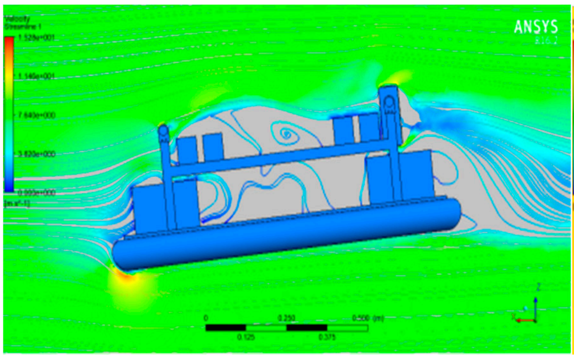

Figure 8, Velocity streamline at 4° AoA

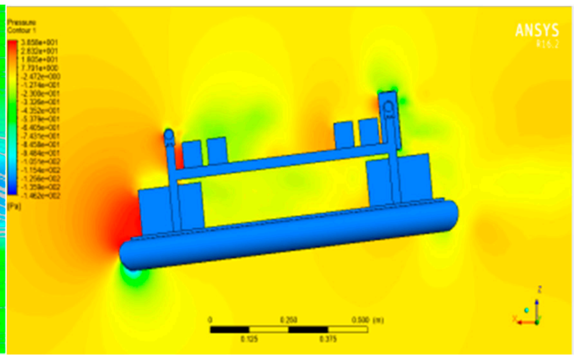

Figure 9, Pressure contour at 4° AoA

For various angles of attach, co-efficient of drag is estimated and corresponding drag force is calculated (Table 11). It is evident that substantial drag is experienced which reduces endurance of UAV. In order to reduce the effect of drag, inclined front panel (Figure 10) and blended nose configurations (Figure 11) are considered.

Table11, Drag Estimation

α Angle of Attack	C_d Drag Coefficient	D Drag (N)
0^0	5.89	38.3
4^0	5.65	36.8
8^0	5.50	35.8

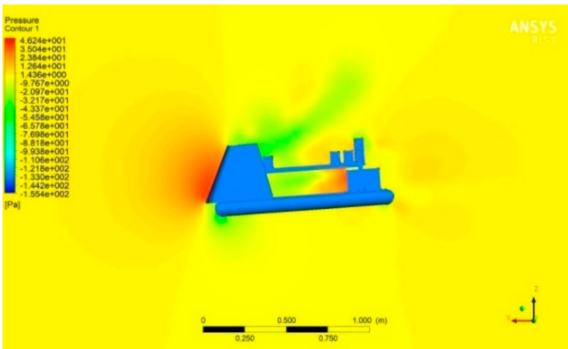

Figure 10, Flat panel - Pressure contour

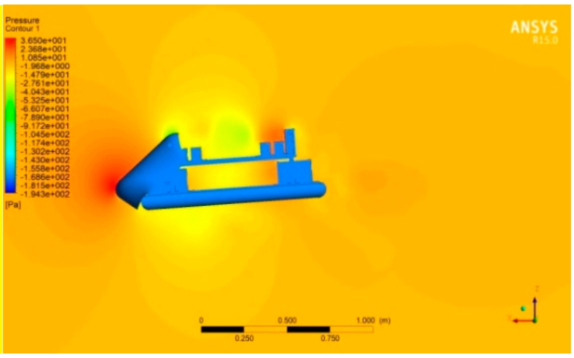

Figure 11, Blended nose - Pressure contour

6. Water sample collection using robotic arm

A 2 degree of freedom (DOF) manipulator actuated using servo motor is used to collect water samples as shown in Figure 12. End–effector carries a water sucking pump which in turn connected through a hose. Drawn water is collected in the respective storage tank of 1 litre capacity. The depth of water collection is controlled using a rope drive through a stepper motor. Encoder feedback is sent to Arduino based controller to monitor the depth of collection of water. The arm of robot manipulator is made up of carbon fibre and water proof servo motor is attached at each link of the robotic arm. During water sample collection, stability of the vehicle is assured through distributing water using a two way control value. Water level sensor is used to measure the quantity of water and corresponding feedback is sent to control the pump and retraction of robotic arm. Buffer plates are placed in the water storage tank to dampen the vibration caused due to turbulence of water in the storage tank.

Preprints (www.preprints.org) | NOT PEER-REVIEWED | Posted: 18 September 2018 doi:10.20944/preprints201809.0326.v1

Peer-reviewed version available at *Sensors* **2018**, *18*, 3318; doi:10.3390/s18103318

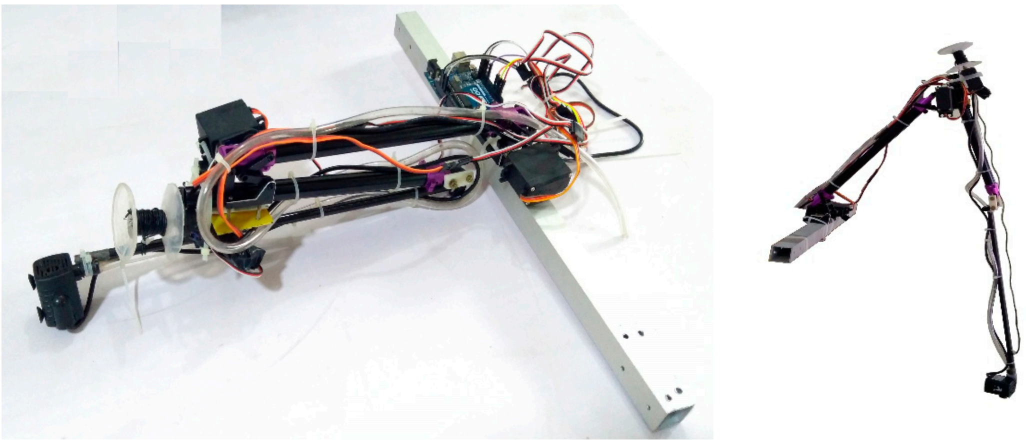

Figure 12, Robotic arm with suction pump assembly

Figure 13, illustrates the payload control unit in which pulse width modulated (PWM) signals are sent to actuate the servo motors. Water level sensors, water quality monitoring sensors, pump, and encoder are used to provide feedback in analog and digital forms.

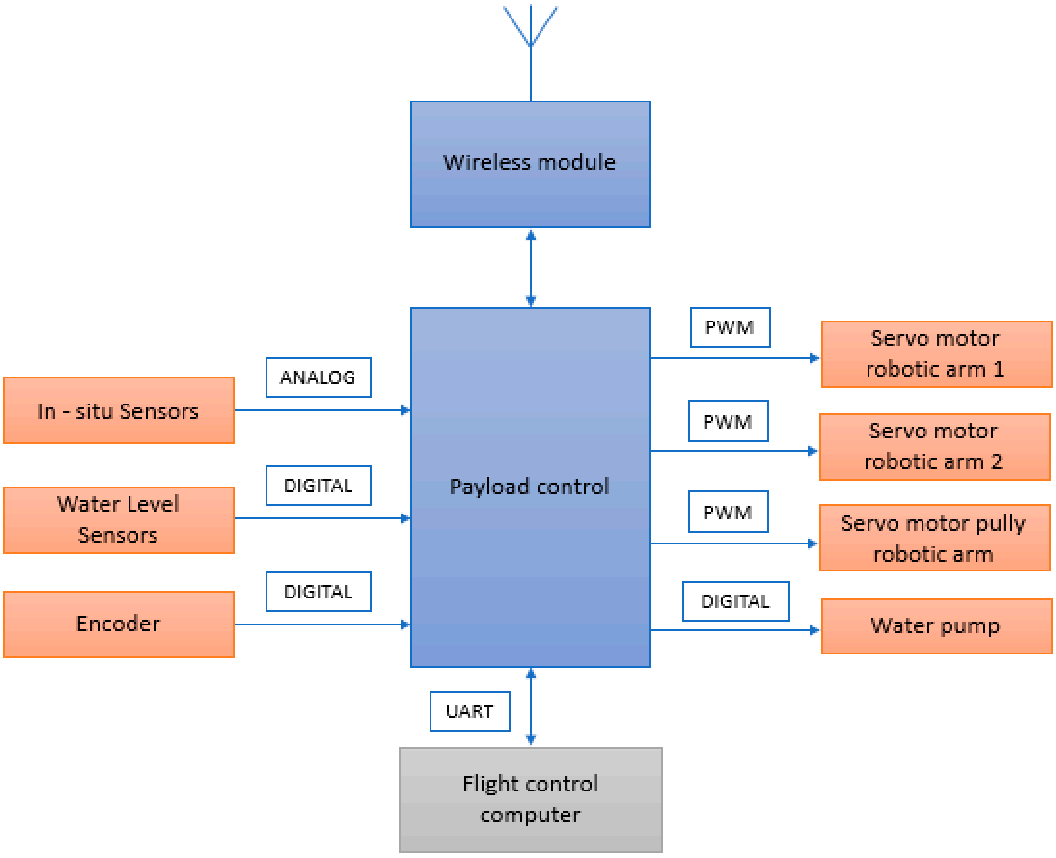

Figure 13, Main control unit

7. Development of ground control station

The ground control station (Figure 14) consist of a portable computer with payload control, mission management and flight data monitoring with corresponding communication links. The mission of amphibious vehicle is pre-planned in the ground control station wherein, vehicle is flown as multi rotor to identify contaminated regions of water body and on-line video is streamed using 5.8GHz video data link. Once contaminated regions are identified, the vehicle is landed on water surface through hover craft mode. Water samples are collected using a robotic arm with suction

Peer-reviewed version available at *Sensors* **2018**, *18*, 3318; doi:10.3390/s18103318

pump and rope mechanism structure. Radio frequency signals in universal asynchronous receiver - transmitter (UART) carrier mode are used to communicate and actuate the servos, sensors and other actuators to collect required water samples with precise feedback.

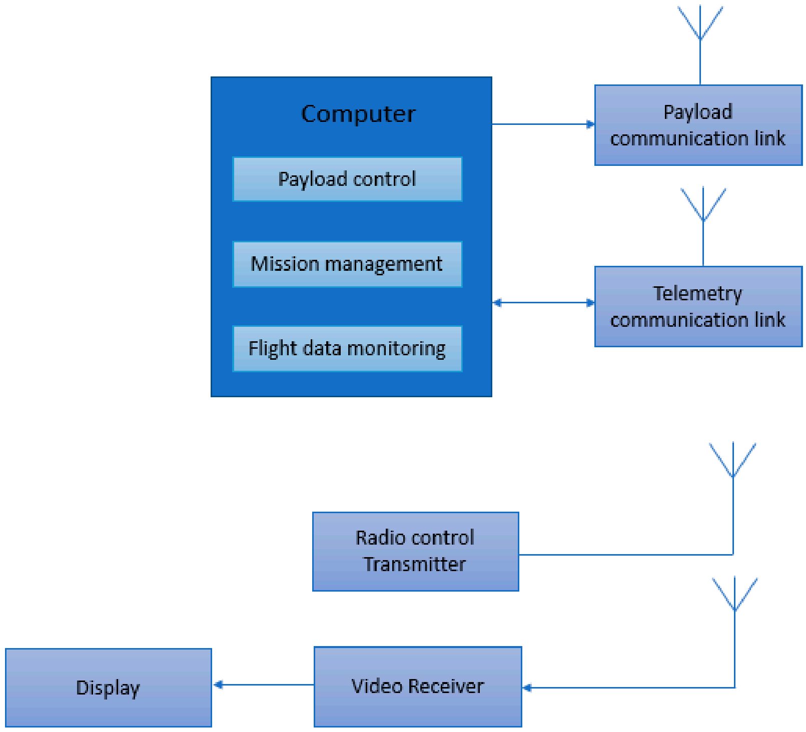

Figure 14, Ground control station

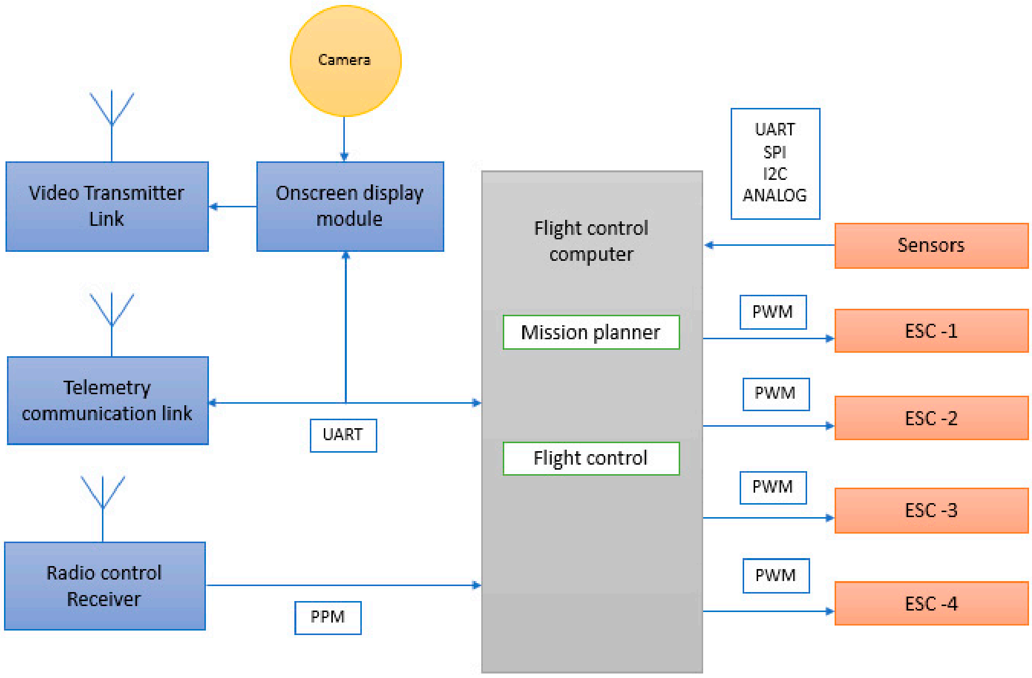

Figure 15, Flight control computer module

A typical flight control computer is presented in Figure 15. It will act as central hub of system through which position, orientation and heading direction of the vehicle are controlled. In addition, the receiving and transmission of data, battery power monitoring, and actuation of servos, motors and robotic arm are performed.

Preprints (www.preprints.org) | NOT PEER-REVIEWED | Posted: 18 September 2018 doi:10.20944/preprints201809.0326.v1

Peer-reviewed version available at *Sensors* **2018**, *18*, 3318; doi:10.3390/s18103318

The airborne mode of mission is depicted in Figure 16 describes that radio frequency signals at 2.4GHz are transmitted and received through telemetry modules. The received signals are sent in pulse position modulated (PPM) form to the flight controller. The flight controller computer handles control and navigation of the vehicle during flying and hovering modes. PWM signal from flight control computer is sent to the electronic speed controller (ESC) to actuate the brushless direct current (BLDC) motor to lift and navigate the vehicle in the desired attitude and altitude. The on-line video streaming is achieved through RF mode and on-screen display module is integrated to monitor the water surface in real time during flying mode. Autonomous capability is achieved through way point navigation, guidance and control with prior mission planning.

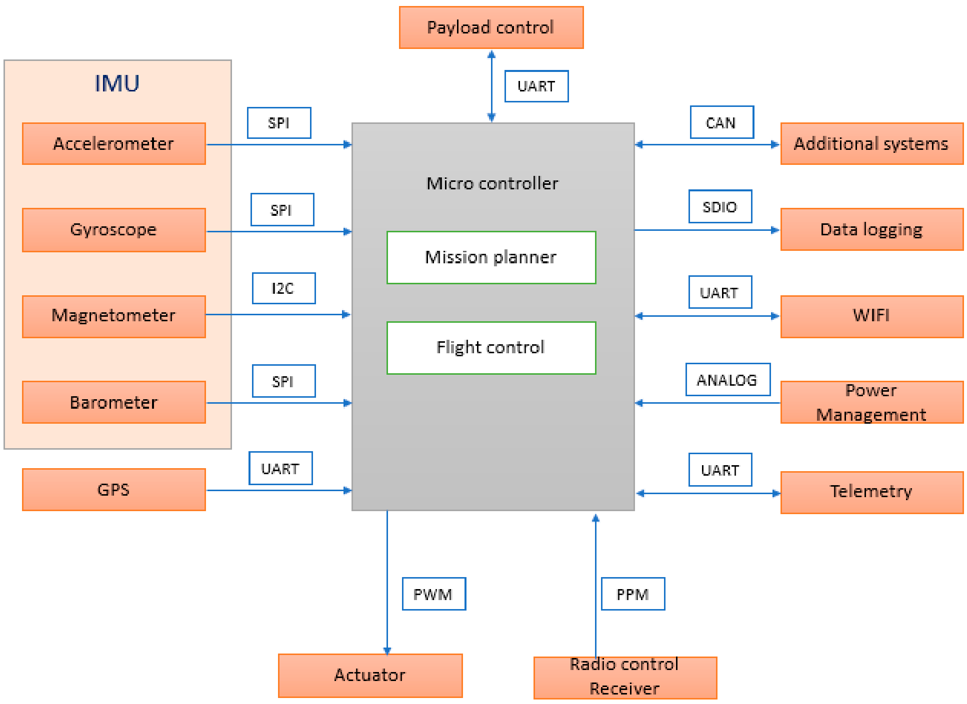

Figure 16, Airborne mission

Preprints (www.preprints.org) | NOT PEER-REVIEWED | Posted: 18 September 2018 doi:10.20944/preprints201809.0326.v1

Peer-reviewed version available at Sensors 2018, 18, 3318; doi:10.3390/s18103318

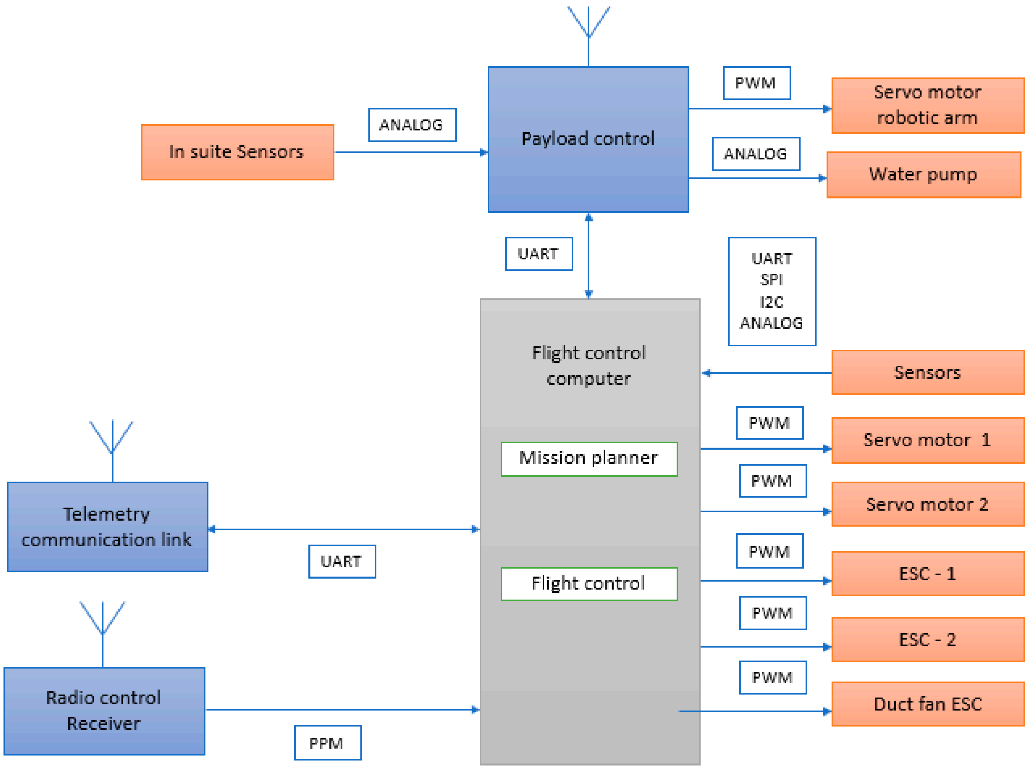

Figure 17, Water sampling mission

During hover mode of vehicle (Figure 17), the pay load control unit is triggered to actuate the robotic arm, water pump and water quality sensors to collect water samples and perform in-situ water quality analysis.

8. Fabrication and assembly of amphibious structure

An amphibious vehicle structure is fabricated (Figure 18) based upon the selected motors, propellers, battery, hull and skirt materials. On top of the hull, vertical hollow aluminum frames are mounted upon which horizontal frames are fixed. At the four corners of horizontal frame, 3D printed knuckle joints are used and motor-propeller configuration is mounted on it. A servo motor is attached to rotate the motor-propeller configuration. At the center of the hull, a propeller is mounted which produces necessary pressure to lift the vehicle through inflating the skirt. An open source advanced level controller is utilized to control and navigate the vehicle. The constructed amphibious vehicle is tested in an ambient environment and stable flight is observed (Figure 19a). Preliminary testing of the vehicle is also taken up in a water tank (Figure 19b) and water is collected through actuating the suction pump.

Figure 18, Prototype of amphibious UAV

(a) (b)

Figure 19, Field testing of Amphibious UAV: (a) Amphibious UAV (Air borne); (b) Amphibious UAV (gliding above water)

The folded robotic arm is extended through a servo actuator after landing the vehicle on water surface and a rope mechanism attached with a suction pump is actuated to suck the water at the desired depth of water channel. After performing water borne mission, the robotic arm assembly is retracted to initial folded configuration for compactness and stability of the vehicle.

9. IoT based water quality measurement

It is essential to perform water quality inspection in a regular interval at the water reservoirs such as dams, lakes, rivers and ponds. Collection of water samples in remote water bodies is challenging and time consuming. Traditional methods of collecting water samples using boats is cumbersome and it is very difficult to access remote water locations. In this work, developed amphibian vehicle can measure the water quality using various on-board water quality sensors such as pH, Dissolved oxygen (DO), Electrical conductivity (EC), Temperature and Turbidity. A Raspberry pi zero BCM 2835, 1 GHz ARM 11 core, 512MB of LPDDR2 SDRAM is utilized to process the sensor data and send via 4G dongle –LTE network at 2300 MHz. The IoT setup shown in Figure 20, is embedded into the designed Amphibious UAV and in-situ water quality measurement is performed. The sensor data are sampled at 160 MHz sampling speed using Arduino pro mini and transmitted to the Raspberry pi UART section. The Raspberry pi is connected with 4G LTE dongle, and the UAV is operated with 2.4GHz radio frequency to avoid inference. Each sensor is calibrated and it provides an analog signal (0 - 5 V) with reference to the measurement. The measured analog signal is sent to the embedded computer as a 16bit digital data.

Peer-reviewed version available at *Sensors* **2018**, *18*, 3318; doi:10.3390/s18103318

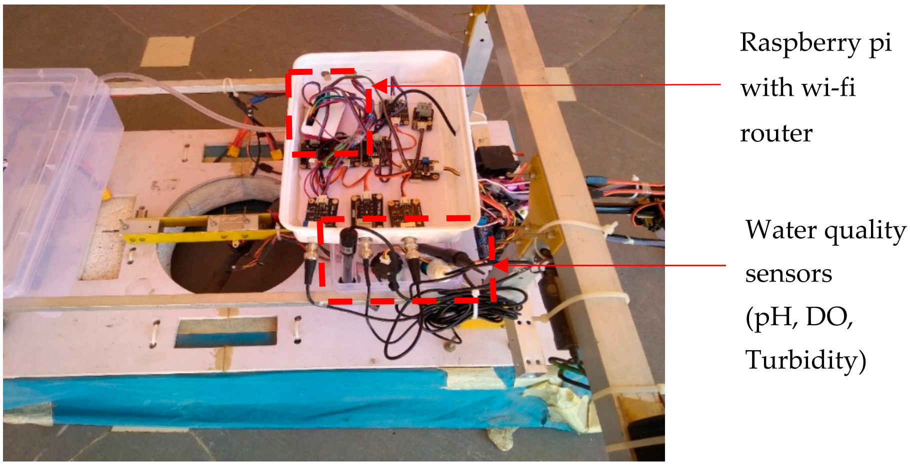

Figure 20, Sensor interface with Raspberry pi

A typical Internet of Things (IoT) based network is shown in Figure 21, demonstrates the working principle of UAV based water quality measurement and transmission of data.

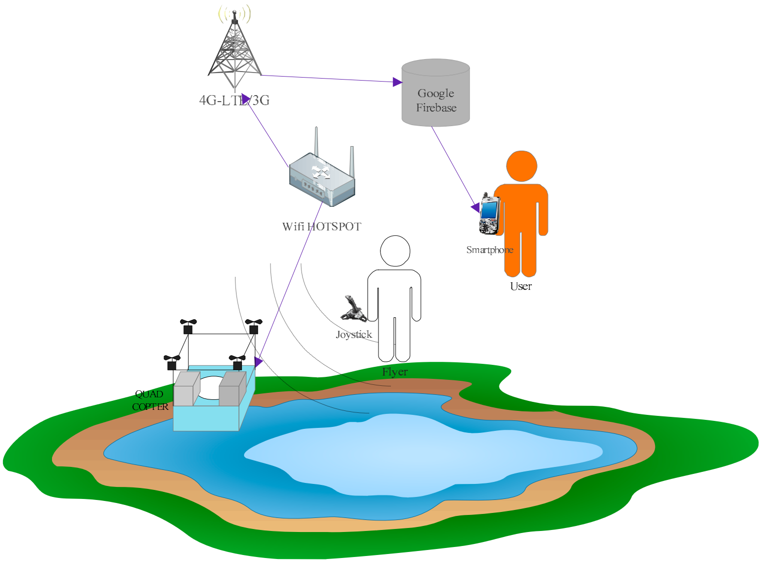

Figure 21, IoT architecture for water quality measurement

The ARM based computer process the sensor data and provide the useful information of measurable quantities in standard units. The water quality information is transferred to the cloud database for real time monitoring and post processing. The link between cloud data base server and real time on-board embedded computer are created with the 4G broadband cellular network because it provides better speed in comparison to 2G and 3G.The water quality data in cloud are accessed through the smart devices with internet service in anywhere in the world. Preliminary experiments are conducted to examine the performance characteristics of sensor network. The saturation time taken for each sensor is obtained and pH took more time to arrive the saturation in comparison with other sensors as shown in Figure 22.

Preprints (www.preprints.org) | NOT PEER-REVIEWED | Posted: 18 September 2018 doi:10.20944/preprints201809.0326.v1

Peer-reviewed version available at *Sensors* **2018**, *18*, 3318; doi:10.3390/s18103318

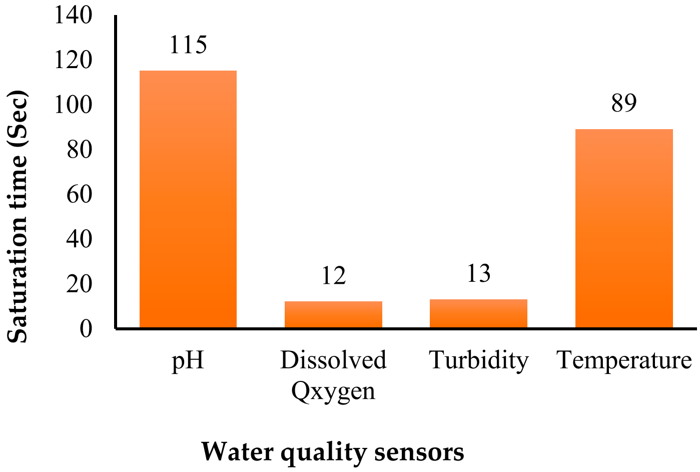

Figure 22, Sensor saturation time

The average delay (500 set transmissions) in water quality data is monitored with different network conditions (4G, 3G and 2 G). The round-trip delay time seems to be better for 4G-LTE communication and it took 11 seconds' in an average to reach the destination (Figure 23).

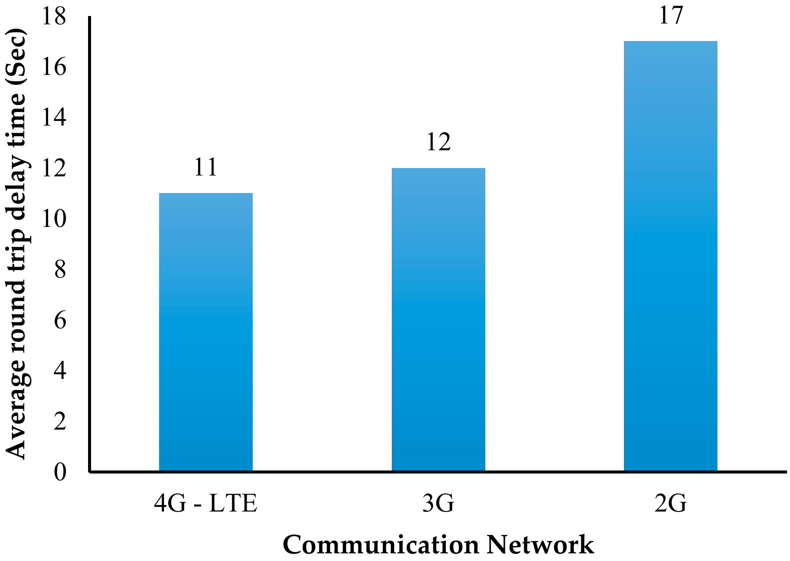

Figure 23, Round trip time

In addition, power consumption of various sensors, transmitting and receiving unit is calculated and it is shown in Figure 24.

Preprints (www.preprints.org) | NOT PEER-REVIEWED | Posted: 18 September 2018 doi:10.20944/preprints201809.0326.v1
Peer-reviewed version available at Sensors 2018, 18, 3318; doi:10.3390/s18103318

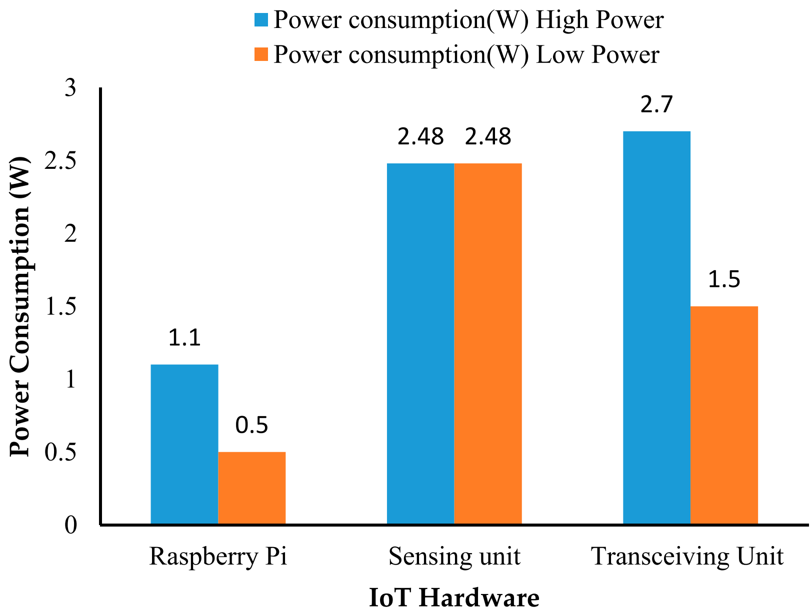

Figure 24, Power consumption of IoT system

The transmitted sensor data is collected in the Google firebase cloud as shown in Figure 25 and it can be synchronized with cloud messaging service and shared across the globe through firebase cloud services.

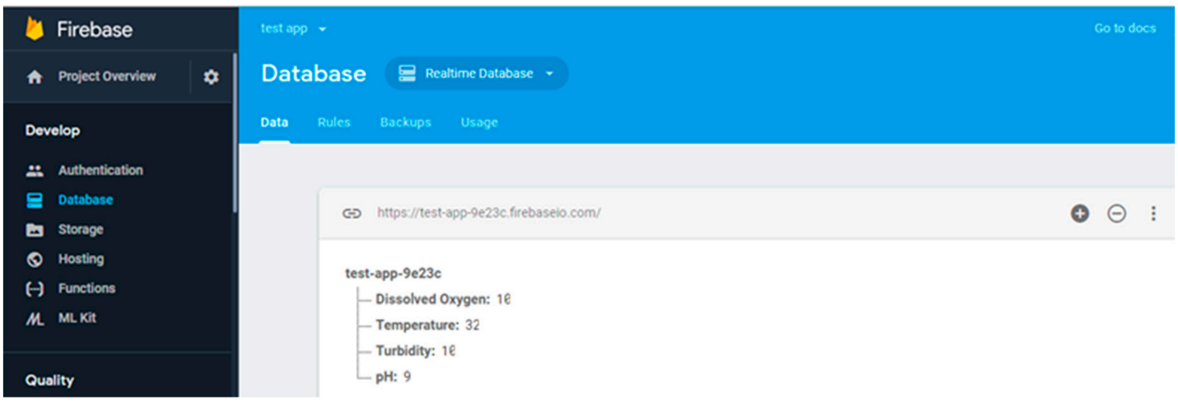

Figure 25, Google fire database

Water quality analysis is performed using various sensors shown in Figure 26. Water sample is collected at a typical lake near to Ambattur, Chennai, India (13°06'27.9"N 80°08'42.0"E) extends over an area approximately 1.57 km² and has a total length of 6.06 km. A Robotic arm with a water sucking pump is used to collect the water and stored in a container. The complete sensor module is isolated to avoid interference of the signal and their probes are immersed into the container. The real time data is transmitted for a period of time until saturation occurs. The measured data is compared with their upper limit (Table 12) based on the IS 10500 water quality standards. It is observed that, the lake water is of poor quality and it needs water treatment to improve the quality of water.

Preprints (www.preprints.org) | NOT PEER-REVIEWED | Posted: 18 September 2018 doi:10.20944/preprints201809.0326.v1

Peer-reviewed version available at Sensors 2018, 18, 3318; doi:10.3390/s18103318

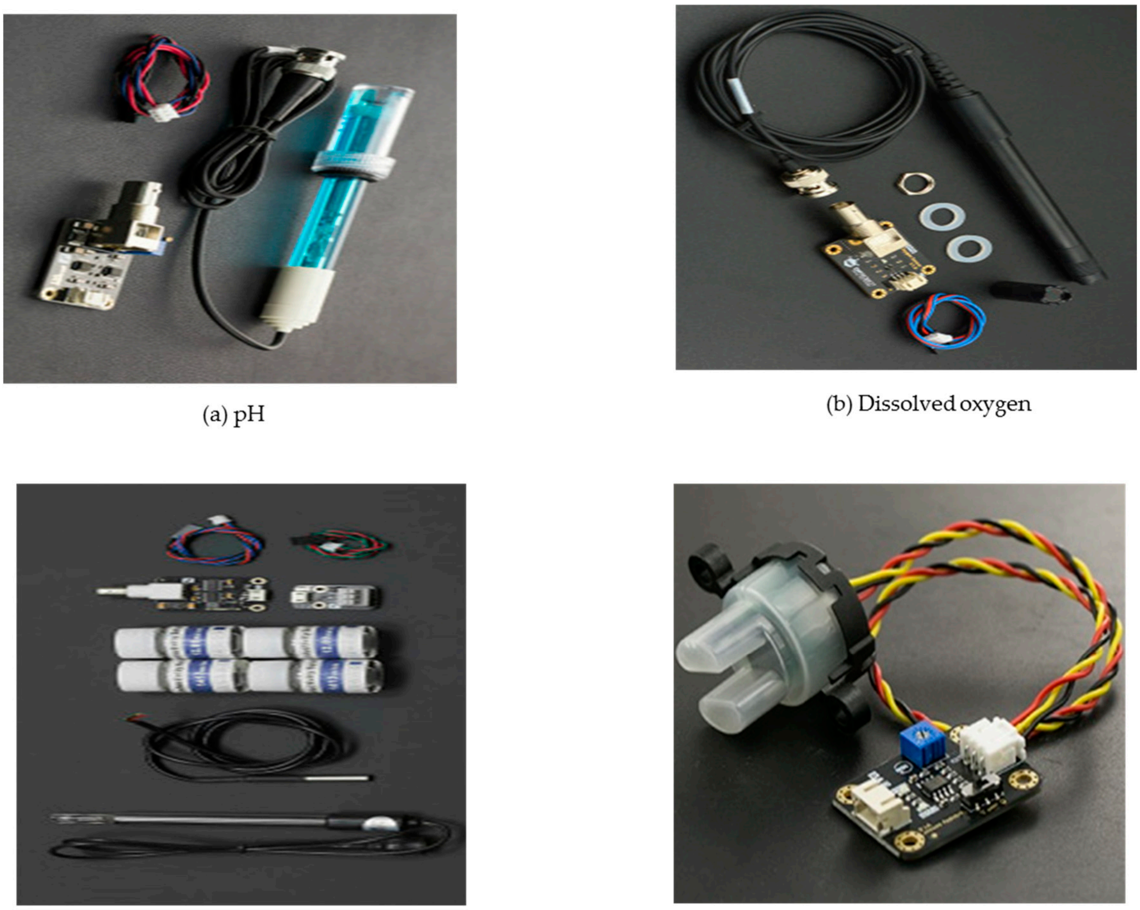

(a) pH (b) Dissolved oxygen

(c) Electrical conductivity (d) Turbidity

Figure 26, Water quality sensors

Table 12, Comparison of water quality with reference to IS 10500 standards

SI.No	Sensors	Results	MaximumAllowable limit	Remark
1	pH	6.06	(acceptable range = 6.5 to 8.5) 7.0+ = alkalinity 7.0 - = acidity	Below thelimit
2	Turbidity (NTU)	8.47	5.0	Above the limit
3	Electric conductivity(ms/cm)	12.73	0 -0.5 mS/cm Good 0.5 - 1.5 mS/cm Normal >1.5 mS/cm High	Above the limit
4	Dissolved oxygen (mg/l)	8.34	Above 6mg/l	Above the limit

10. Conclusion

An amphibious vehicle is developed for achieving a mission endurance of 25 minutes while carrying a payload of 7kg. Design of the vehicle combines the functionalities of multi-rotor UAV and a hovercraft. Through engineering analysis and simulations, performance of the vehicle is evaluated with reference to deformation, stresses, forward velocity and stagnation pressure corresponding to expected operational conditions. Appropriate selection of materials for obtaining superior strength characteristics, motors and propeller to generate sufficient thrust forces and considering 2 DOF robotic arm integrated with water sucking pump, a prototype is built and tested in airborne condition (open field) and also in a water body to evaluate the stability and response. The developed amphibious system is able to collect water samples of 500 ml through actuating the suction pump attached at the end-effector of the robotic arm.IoT based water qulaity analysis revealed that within 11 milliseconds 4G – LTE network tranmitted the data to the ground station throgh firebase cloud services. The developed IoT hardware unit consumed 7.58W power andeach sensor saturation limitis meaured. pH sensor consumed 115 sec to reach saturation and dissolved oxygen required 12 sec to attain saturation of sensed data. Water quality analysis results suggested that as per IS 10500 water quality standards the inspected lake water is having impurity which may not be suitable for drinking purpose.

Acknowledgement: Authors would like to thank the funding supported by NRF Korea-India Science and Technology Cooperation Expansion Project (NRF – 017K1A3A1A57093906) and the DGIST R & D program of the Ministry of Science and ICT (18-IT-02, 20180463) and also from DST – GITA (Ref: 2015RK0201103).

Author Contributions: Balasubramanian Esakki developed the conceptual design of amphibious vehicle, finite element analysis and prepared the entire manuscript, Surendar Ganesan calculated the motor, propeller and hovercraft system parameters using empirical relations, design calculations and computational fluid dynamic analysis, Silambarasan Mathiyazhagan andBhuvaneshwaran Gnanasekaran involved in the prototype development, testing of amphibious vehicle and water quality analysis, Kanagachidambaresan and Jae Sung Choi formulated IoT protocols and real time performance testing, Su Woo Park and Byungrak Son designed robotic arm for water sampling and water quality analysis using various sensor modules.

Conflicts of Interest: The authors declare no conflict of interest.

References

1. Valavanis, K. P.;& Vachtsevanos, G. J. (2015). Future of unmanned aviation. In Handbook of unmanned aerial vehicles (pp. 2993-3009). Springer, Dordrecht.
2. Hassanalian, M.;& Abdelkefi, A. B. (2017). Classifications, applications, and design challenges of drones: a review. Progress in Aerospace Sciences, 91, 99-131.
3. Prakash, N. U.; Vasantharaj, R.; Balasubramanian, E.; Bhushan, G.; Das, S.;& Eqbal, F. (2014). Design, development and analysis of air mycoflora using fixed wing unmanned aerial vehicle (UAV). Journal of Applied Science and Engineering, 17(1), 1-8.
4. Sankarasrinivasan, S.; Balasubramanian, E.; Karthik, K.; Chandrasekar, U.;& Gupta, R. (2015). Health monitoring of civil structures with integrated UAV and image processing system. Procedia Computer Science, 54, 508-515.
5. Yang, L. J.; Esakki, B.; Chandrasekhar, U.; Hung, K. C.;& Cheng, C. M. (2015). Practical flapping mechanisms for 20 cm-span micro air vehicles. International Journal of Micro Air Vehicles, 7(2), 181-202.
6. Udayagiri, C.; Kulkarni, M.; Esakki, B.; Pakiriswamy, S.;& Yang, L. J. (2016). Experimental Studies on 3D Printed Parts for Rapid Prototyping of Micro Aerial Vehicles. Journal of Applied Science and Engineering, 19(1), 17-22.
7. Chandrasekhar, U.; Yang, L. J.; Esakki, B.; Suryanarayanan, S.;& Salunkhe, S. (2017). Rapid prototyping of flapping mechanisms for monoplane and biplane ornithopter configurations. International Journal of Modern Manufacturing Technologies 9 (2), 18-22.
8. Collins, K. A. (1993). A concept of unmanned aerial vehicles in amphibious operations (Doctoral dissertation, Monterey, California. Naval Postgraduate School).
9. Boxerbaum, A. S.; Werk, P.; Quinn, R. D.;& Vaidyanathan, R. (2005, July). Design of an autonomous amphibious robot for surf zone operation: Part I mechanical design for multi-mode mobility. In Proceedings, 2005 IEEE/ASME International Conference on Advanced Intelligent Mechatronics. (pp. 1459-1464). IEEE.

10. Yayla, M.; Sarsilmaz, S. B.; Mutlu, T.; Cosgun, V.; Kurtulus, B.; Kurtulus, D. F.;& Tekinalp, O. (2013). Dynamic Stability Flight Tests of Remote Sensing Measurement Capable Amphibious Unmanned Aerial Vehicle (A-UAV). AIAC, 7th Ankara International Aerospace Conference, Ankara, Türkiye.
11. Pisanich, G.;& Morris, S. (2002). Fielding an amphibious UAV: development, results, and lessons learned. In Digital Avionics Systems Conference, 2002. Proceedings. The 21st (Vol. 2, pp. 8C4-8C4). IEEE.
12. Hasnan, K.;& Ab Wahab, A. (2012). First Design and Testing of an Unmanned Three-mode Vehicle. International Journal on Advanced Science, Engineering and Information Technology, 2(1), 13-20.
13. Frejek, M.;& Nokleby, S. (2008, May). Design of a small-scale autonomous amphibious vehicle. In Electrical and Computer Engineering, 2008. CCECE 2008. Canadian Conference on (pp. 000781-000786). IEEE.
14. Amyot, J. R. (Ed.). (2013). Hovercraft technology, economics and applications (Vol. 11). Elsevier.
15. Koko, M. I. A. A. (2014). Design of a Typical Multi-Role Vehicle Using Quad-Rotor Theory (Doctoral dissertation, Sudan University of Science and Technology).
16. Detweiler, C.; Griffin, B.;& Roehr, H. (2012, October). Omni-directional hovercraft design as a foundation for MAV education. In Intelligent Robots and Systems (IROS), 2012 IEEE/RSJ International Conference on (pp. 786-792). IEEE.
17. Schleigh, J. (2006). Construction of a Hovercraft Model and Control of its Motion (Doctoral dissertation).
18. Rashid, M. Z. A.; Aras, M. S. M.; Kassim, M. A.; Ibrahim, Z.;& Jamali, A. (2012). Dynamic Mathematical Modeling and Simulation Study of Small Scale Autonomous Hovercraft. International Journal of Advanced Science and Technology, 46, 95-114.
19. Fuller, S. B.;& Murray, R. M. (2011, December). A hovercraft robot that uses insect-inspired visual autocorrelation for motion control in a corridor. In Robotics and Biomimetics (ROBIO), 2011 IEEE International Conference on (pp. 1474-1481). IEEE.
20. Amiruddin, A. K.; Sapuan, S. M.;& Jaafar, A. A. (2011). Development of a hovercraft prototype with an aluminium hull base. International Journal of Physical Sciences, 6(17), 4185-4194.
21. Haider, A.;& Sajjad, M. (2012). Structural design and non-linear modeling of a highly stable multi-rotor hovercraft. Control Theory and Informatics, 2(4), 24-35.
22. Frejek, M.;& Nokleby, S. (2008, May). Design of a small-scale autonomous amphibious vehicle. In Electrical and Computer Engineering, 2008. CCECE 2008. Canadian Conference on (pp. 000781-000786). IEEE.
23. Weerasinghe, R.;& Monasor, M. (2017). Simulation and experimental analysis of hovering and flight of a quadrotor.
24. Ozdemir, U.; Aktas, Y. O.; Vuruskan, A.; Dereli, Y.; Tarhan, A. F.; Demirbag, K.;& Inalhan, G. (2014). Design of a commercial hybrid VTOL UAV system. Journal of Intelligent & Robotic Systems, 74(1-2), 371-393.
25. Kuantama, E.; Craciun, D.;& Tarca, R. (2016). Quadcopter Body Frame Model and Analysis. Annals of the University of Oradea, 71-74.